Numerical simulation of the 3ω method for measuring the thermal conductivity

A. Jacquot, Bertrand Lenoir, A. Dauscher, M. Stölzer, J. Meusel

Numerical simulation of the 3ω method for measuring the thermal conductivity

Cite as: Journal of Applied Physics **91**, 4733 (2002); https://doi.org/10.1063/1.1459611
Submitted: 08 March 2001 • Accepted: 09 January 2002 • Published Online: 28 March 2002

A. Jacquot, B. Lenoir, A. Dauscher, et al.

Numerical simulation of the 3ω method for measuring the thermal conductivity

A. Jacquot,[a] B. Lenoir, and A. Dauscher
Laboratoire de Physique des Matériaux, UMR CNRS-INPL-UHP 7556, Ecole des Mines, Parc de Saurupt, F-54042 Nancy, France

M. Stölzer and J. Meusel
Martin-Luther-Universität Halle, FB Physik, D-06099 Halle, Germany

(Received 8 March 2001; accepted for publication 9 January 2002)

A four-pad 3ω method was developed for determining the thermal conductivity of bulk and thin film materials. The heat conduction in the sample geometry was investigated by numerical simulation employing the finite volume technique. As a result, the conditions (i.e., sample geometry, frequency range) can be predicted when conventional analytical formulas are suited to determine the thermal conductivity of bulk and thin film material from the data measured. Experiments were performed that confirm the validity and accuracy of the numerical calculations. © *2002 American Institute of Physics.* [DOI: 10.1063/1.1459611]

I. INTRODUCTION

The thermal conductivity in thin-film structures has received particular attention in recent years in both fundamental and applied research.[1–17] The thermal properties of these low-dimensional structures are basically involved in several applications, such as in small-scale thermoelectric devices or electronic, and optoelectronic devices. Understanding the heat diffusion mechanisms as well as a careful thermal design of these devices is becoming increasingly important for improving their performance and reliability. Therefore, the thermal conductivity is crucial information. But to date it suffers from a lack of experimental data arising from difficulties in the measurement.

Standard measurement techniques used for bulk materials, e.g., the steady-state method where a heater is connected at one end of the sample while the other end is in good thermal contact with a heat sink, are particularly impractical for measuring thin films, because of the substantial heat losses through the substrate and/or by radiation. Among the variety of experimental methods developed to measure the thermal conductivity of thin films, the technique referred to as the 3ω method[18] has yielded the most accurate data for cross-plane characterization. This dynamic technique uses a thin metal strip on the surface of the sample acting as both an electrical heater and a thermometer. A sinusoidal current of frequency ω is applied and the measurements are performed within a frequency range. The use of an ac current allows for working with relatively small sample volumes because the reach of the thermal waves inside the sample is far smaller than the reach of a steady temperature field.

The 3ω method was initially developed for thermal conductivity measurements of amorphous bulk materials exhibiting low thermal conductivity values.[19] It was then intensively applied to determine the cross-plane thermal conductivity of films, ranging from nanometers to micrometers in thickness, deposited on high thermal conductivity substrates, and furthermore to superlattices.[5–12,20,21] Attempts to extract the in-plane thermal conductivity were also considered using this technique.[10,11,22]

Although the method was extended to more complex samples, the data analysis was still undertaken using the analytical formulas proposed by Cahill *et al.*[6,18] which were derived under binding hypotheses such as the semi-infinite size of the sample and the infinite length of the heater. It would be of great interest to predict the conditions for which these analytical formulas are appropriate and to complete previous developments in the case of a real sample of limited size. These problems were already investigated by the finite element technique in 3ω sensors used in dynamic heat capacity measurements.[23] A similar approach would be highly desirable in the case of thermal conductivity.

In this article, numerical simulations of the 3ω method based on the finite volume technique are presented. These simulations take into account the geometry of the strip, the sample boundary conditions (i.e., isothermal or adiabatic) and the thermal properties of both the heater and the sample under investigation. Consequently, the influence of these factors on the experimental results can be studied. The results of the numerical simulation will be compared to experimental data obtained on a thick Kapton foil sample and on a SiO_2 layer on a silicon substrate.

II. STATE OF THE ART

A. Principles of the 3ω method

A narrow metal strip of width $2b$ (typically $2<2b<100\ \mu$m) and length l, with two or four pads, is prepared on the sample surface using generally thermal evaporation and photolithography (Fig. 1). An ac driving current, $I=I_0\cos(\omega t)$, heats the metal strip and the sample at frequency 2ω. Due to the temperature rise of the strip $\Delta T=\Delta T_0\cos(2\omega t+\varphi)$, the resistance R varies as $R=R_0(1+\alpha\Delta T)$, where $\alpha=1/R(dR/dT)$, and oscillates also at a

[a]Electronic mail: alexandre.jacquot@lpm.u-nancy.fr

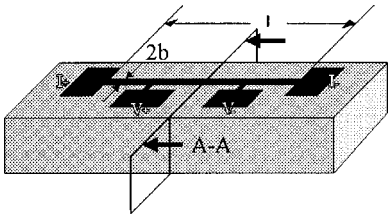

FIG. 1. Geometry of the four-pad 3ω method. A metal strip serves as both the heater and the thermometer. The four pads are the connections for current leads (I_+,I_-) and voltage leads (V_+,V_-). l is the distance between the current leads, $2b$ is the strip width, and A-A the cross section of the sample.

frequency 2ω. With regard to the frequency used in the heater, the phase shift φ depends on both the geometry of the heater and the thermal properties of the medium. According to Ohm's law, the voltage drop $V=RI$ measured across the metal strip is amplitude-modulated and has a small component at the third harmonic 3ω:

$$V=R_0 I_0 \cos \omega t+\frac{R_0 I_0}{2}\alpha \Delta T_0 \cos(\omega t+\varphi)$$

$$+\frac{R_0 I_0}{2}\alpha \Delta T_0 \cos(3\omega t+\varphi). \tag{1}$$

The third harmonic in Eq. (1) can be extracted from the total signal using a lock-in amplifier and can be used to measure ΔT_0 and the phase shift φ, if α is known.

B. Temperature rise: Analytical formulas

In the case of a strip deposited on an insulating material, Cahill[18] has shown that the complex temperature rise $\Delta \tilde{T}$ at the heater can be calculated from

$$\Delta \tilde{T}=\frac{P_1}{\pi \lambda}\int_0^\infty \frac{\sin^2(kb)}{(kb)^2(k^2+q^2)^{1/2}}dk, \tag{2}$$

where P_1 is the heating power input to the strip per unit of length, λ is the thermal conductivity of the sample under investigation, and $|1/q|$ is the wave penetration depth (WPD) defined by

$$\left|\frac{1}{q}\right|=\sqrt{\frac{\lambda}{2\rho c_p \omega}}, \tag{3}$$

where ρ and c_p are the density and the specific heat per unit volume of the material, respectively.

Equation (2) is based on the assumptions that the strip thickness can be neglected, the strip length is infinite [two-dimensional (2D) heat flow], the sample size is semi-infinite, and the thermal conductivity of the material is isotropic.

When the WPD is large compared to the strip width, Eq. (2) can be well-approximated by[18]

$$\Delta \tilde{T}=\frac{P_1}{\pi \lambda}\left[-\frac{1}{2}\ln(2\omega)+\frac{1}{2}\ln\frac{\lambda}{\rho c_p b^2}+\eta-i\frac{\pi}{4}\right], \tag{4}$$

where η is a constant.

This analytical formula resulted in the thermal conductivity of the studied material that can be extracted either from the slope of the in-phase temperature rise versus $\ln(2\omega)$ plot, or from the out-of-phase component. In practice, the first approach is generally used because of its better accuracy.

For a film-on-substrate sample, the total temperature rise at the heater is composed of two parts: one is the temperature rise in the substrate and the other is the temperature drop across the film. If the metal line is wide compared to the thickness of the film, the heat flow in the film will be mainly in the cross-plane direction, and the film simply adds a frequency–independent thermal resistance[7]

$$\Delta T_f=\frac{P_1 e}{2b\lambda_f}, \tag{5}$$

where e is the thickness and λ_f is the cross-plane thermal conductivity of the film.

This approach requires that the thermal conductivity of the film must be much smaller than that of the substrate. Note that in this case the accuracy of the measurement is highly dependent on the accuracy of the strip dimensions.

By reducing the heater width, the heat flow becomes 2D because of significant heat flow in the in-plane direction. Therefore, using two metal strips of different width, the in-plane and the cross-plane thermal conductivity values can be obtained.[10,11,22]

If the thermal conductivity of an electrical conducting film has to be investigated, an additional insulating layer between the film and the metal strip is required. The system under consideration now consists of the substrate, two continuous films, and the metal strip.

III. NUMERICAL SIMULATION

We have solved the time-dependent heat transfer problem of a 3ω -experiment by a numerical simulation technique based on the finite volume method. The general problem should be solved using a three-dimensional (3D) grid. However, in the case of a very long metal strip, it can be reduced to a 2D problem, considering only a plane perpendicular to the strip. Because of the high computational power required, we used the 3D model only for investigating the influence of a limited strip length, whereas all calculations of real sample geometries where carried out in 2D only. In particular, the influence of the finite sample size, heater heat capacitance, and heat spreading inside the heater has been considered.

Figure 2 shows the grids used in the calculations. In 2D geometry [Fig. 2(a), cartesian coordinates], the heat flows in a plane normal to the axis **n** of the strip. In 3D geometry [Fig. 2(b), cylinder coordinates], the strip is assumed to be a rod with a finite diameter. In both cases, a temperature field will be obtained at each time step.

The simulation takes place on half of a sample cross-section area (cross section A-A, Fig. 1) and a quarter of a cylinder in 2D and 3D geometry, respectively. The area (2D geometry) and the volume (3D geometry) are typically divided into 900 cells (Fig. 2). In each cell, a linear equation is derived from the condition that the sum of all heat fluxes coming in, coming out, being stored and created is zero. All these equations form a matrix that is solved with an iterative process based on Gauss–Seidel method.

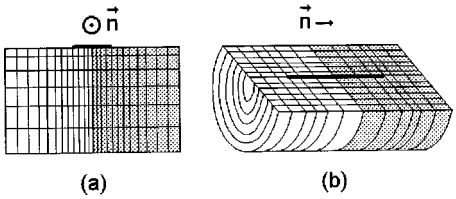

FIG. 2. Geometry of the models used in the numerical simulations to solve the heat transfer problem in (a) 2D and (b) 3D. Due to the symmetry, the analysis is reduced to a half cross section in 2D and to a quarter of a cylinder in 3D (gray parts). In 3D, the strip is assumed to be a rod. Note that the density of cells near the heater or the end of the strip is higher to better calculate the temperature distribution.

Each temperature oscillation is typically divided into 200 time steps. The steady amplitude of temperature oscillation is reached after about three temperature oscillations. In 2D simulation, the boundary conditions are adiabatic at the symmetry line, isothermal at the right border, and finally either isothermal or adiabatic at the bottom of the sample (Fig. 3). Assuming an isothermal boundary condition means the sample is mounted on a perfect heat sink whereas assuming an adiabatic boundary condition simulates a bad thermal contact between the sample and sample holder. For the simulations performed in 3D geometry, a constant temperature is assumed on the surface of the cylinder.

IV. EXPERIMENT

A nickel heater whose geometry is shown in Fig. 1, was sputter deposited on the surface of the sample and patterned by photolithography. Nickel was chosen because of its large temperature coefficient of resistivity. Typically, the strip thickness is about 400 nm, the length l is 4 mm, the distance between the voltage pads is 2 mm and the width $2b$ is 20 μm.

The 3ω experimental setup to measure the thermal conductivity is based on a technology using differential amplifiers (four-pad 3ω method). The signal at frequency ω, free from harmonics, and the voltage containing the 3ω signal are acquired across a reference resistor of low-temperature dependence and the inner pads of the strip, respectively. A differential amplifier is used to increase the ratio of 3ω voltage to 1ω voltage. The resulting signal is digitalized and the 3ω part (amplitude and phase) is extracted by means of numerical lock-in technique. The integration is carried out over typically ten periods. More details of the experimental setup can be found elsewhere.[24]

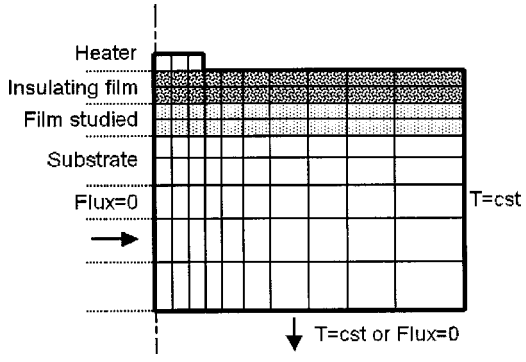

FIG. 3. Cross-sectional view of the grid for a 2D numerical simulation of the thermal conductivity measurement applied to a conducting thin film deposited on a substrate, using the 3ω method. The boundary conditions are adiabatic at the symmetry line, isothermal on the right lateral surface, and either isothermal or adiabatic at the bottom of the sample.

TABLE I. Physical properties of materials used for the simulations according to litterature.[a]

Material	Density (kg m^{-3})	Specific heat [J kg^{-1} K^{-1}]	Thermal conductivity (W m^{-1} K^{-1})
Glass	2500	775	1.1
Silicon	2330	711	148
Kapton	1420	1090	0.32[b]
Silicon dioxyde	2500	775	1.4
Nickel	8900	440	45[c]

[a]Data taken from Refs. 25–28.
[b]Our work.
[c]As the electrical resistivity of the nickel strip is twice its bulk value, the thermal conductivity was fixed to half its bulk value, as a consequence of the Wiedemann-Franz law (see Ref. 29).

Measurements were performed at room temperature on a 125-μm-thick Kapton foil and on a 570-nm-thick thermally grown silica layer on a bare 230-μm-thick silicon wafer. The temperature oscillation amplitude is less than 3 K.

V. RESULTS AND DISCUSSION

A. Effect of a finite strip length

The effect of a finite strip length has been studied by using the cylindrical geometry mentioned before. Two simulations have been performed on two distinct substrates exhibiting a large difference in thermal conductivity: glass and silicon. The thermal properties used in the calculations are mentioned in Table I. The length l was 4 mm as in our measurements. The size of the cylinder considered in the simulation has been chosen such that it does not affect the temperature rise.

The changes of the in-phase temperature oscillation amplitude along the strip are plotted for different frequencies in Figs. 4(a) and 4(c) for glass and silicon, respectively. The in-phase temperature oscillation amplitude averaged over the length of the strip and between the voltage leads is plotted as a function of frequency in Figs. 4(b) and 4(d). The average amplitude over the length of the strip represents the value that is commonly measured using a two-pad geometry, i.e., when the same pads are used for passing the current through the strip and as voltage probes, whereas the average amplitude between the voltage leads represents the value that is measured in a four-pad geometry, i.e., in the geometry of our experiment.

The amplitude drop at the strip ends becomes sharper when the frequency increases from 1 to 1000 Hz, meaning that the heat flow becomes more two-dimensional [Figs. 4(a) and 4(c)]. The agreement between the slope of the curve calculated with Cahill's formula [Eq. (4)] and the slope given by the numerical simulation becomes better when the frequency increases [Figs. 4(b) and 4(d)]. Nevertheless, it should be pointed out that the effect of the finite strip width is neglected in the simulation because of the cylindrical sym-

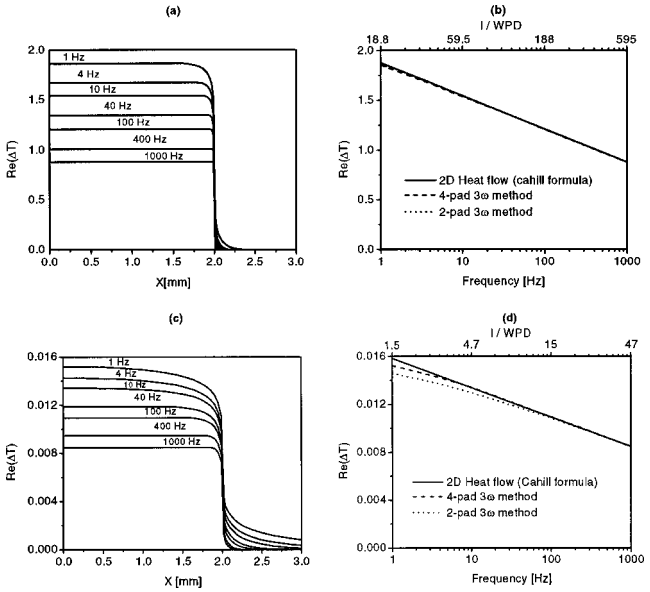

FIG. 4. Effect of a finite strip length on the in-phase ac temperature rise. Modeling for (a), (b) glass and (c), (d) silicon as a function of (a), (c) the distance along the metal strip ($l=4$ mm) for different heater frequencies and (b), (d) the heater frequency. The dotted and dashed curves are obtained by simulating a 3D heat flow, the temperature being averaged along the entire strip and the inner voltage pads, respectively. The solid curves are calculated according to Eq. (4) by adjusting η to fit the calculated curve at high frequencies. The heating power input to the strip per unit length is 1 W m^{-1}. The difference at low frequencies is found to be larger for materials having a high thermal conductivity.

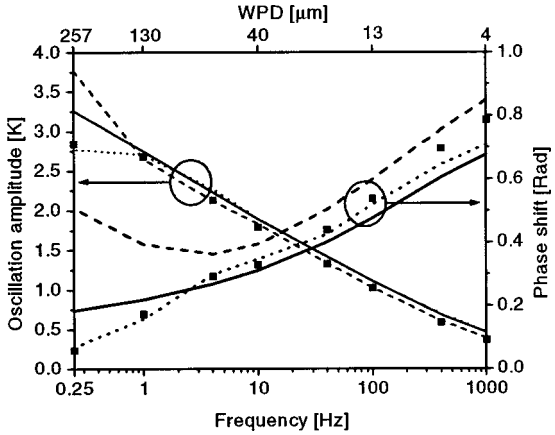

FIG. 5. Measurement and numerical simulation using a heating power per unit length of 0.77 W m^{-1} on a 125-μm-thick Kapton foil. The two arrows separate the oscillation amplitude from the phase shift curves. ■: Experimental points (oscillation amplitude and phase). Dotted lines: amplitude and phase calculated assuming an isothermal boundary condition at the bottom of the sample and neglecting the strip thickness. Dashed lines: amplitude and phase calculated assuming an adiabatic thermal contact at the bottom of the sample and taking into account the strip thickness. Solid lines: calculated amplitude and phase shift using the integral form of Cahill's formula as defined by Eq. (2).

metry used. The wave penetration depth then remains larger than the width of the strip, whatever the frequency is. For silicon, the disagreement with Cahill's formula appears below 10 and 100 Hz in a four- and two-pad geometry, respectively. The discrepancy is as large as 8% at 1 Hz, in a two-pad geometry for silicon [Fig. 4(d)], whereas there is quasi no noticeable discrepancy for glass [Fig. 4(b)] at the same frequency. A slight discrepancy for glass is observed at 1 Hz at a l/WPD ratio of about 18, in the two-pad geometry.

The discrepancy with Si can be understood by comparing the thermal wavelength with the length of the strip. The lower the ratio l/WPD is, the higher the deviation from Cahill's formula is. For Si, the deviation becomes lower than 1%, when l/WPD is larger than 4.7 (10 Hz) in the four-pad geometry and 15 (100 Hz) in the two-pad geometry. It is clear that the use of a four-pad geometry is more suitable to reduce the effect of heat spreading in 3D, as the heat flow tends to be 2D between the inner pads. Note that the effect of heat spreading in 3D is noticeable at roughly the same l/WPD ratio for glass and silicon. For other geometries, it is expected that the discrepancy scales simply with the l/WPD ratio.

In the next parts a two-dimensional heat transfer will be considered only.

B. Influence of boundary conditions

Effects of the finite thickness of both, strip and substrate, are real problems that can affect experimental measurements at both low and high frequency. Although an analytical formula for extracting the thermal conductivity of films on a substrate of finite thickness has been developed,[25] we have investigated the boundary effects numerically and experimentally. The two different types of samples, Kapton and SiO_2 on Si, have been considered again. The Kapton foil was glued on the copper sample holder with silver paint, ensuring a good thermal contact, while the silicon was glued with silicon grease.

For Kapton, measurements were performed between 0.25 and 1000 Hz corresponding to a WPD variation between 260 and 4 μm. The thermal properties of Kapton and nickel used in the calculations are listed in Table I. The thermal conductivity of Kapton used in the numerical simulation was adjusted to fit the experimental data.

The experimental and the simulated amplitude and phase of the temperature rise on the metal strip versus frequency obtained for the Kapton foil are shown in Fig. 5. Rather than the in-phase and out-of-phase components of the temperature rise, the amplitude and phase are used, because they are directly measured and because Eq. (4) is not used to interpret the data. The pair of dotted curves are calculated assuming an isothermal boundary condition and neglecting the thickness of the heater. The pair of dashed curves are calculated assuming an adiabatic boundary condition and taking into account the strip thickness and the heat spreading inside the strip. The pair of solid lines are the amplitude and phase shift calculated from the integral form of Cahill's formula [Eq. (2)].

As shown in Fig. 5, the amplitude of Eq. (2) does not fit the experimental curve very well, especially at low frequencies. In the low-frequency limit (<1 Hz) the assumed isothermal boundary condition at the bottom of the sample agrees well with the experimental data. In this frequency range, the WPD exceeds the sample thickness. As a result, the heat penetrates into the copper sample holder resulting in a decrease of the temperature rise due to its high thermal

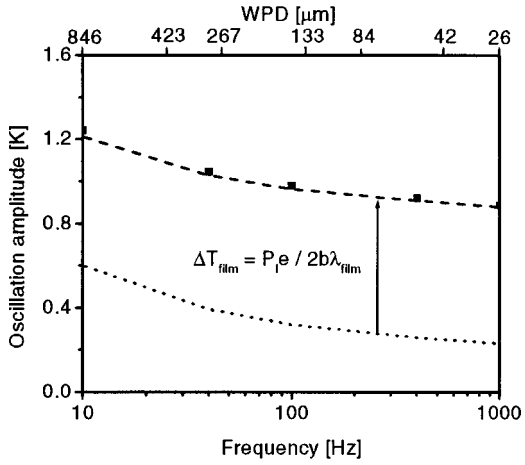

FIG. 6. Measurements on silicon using a heating power per unit length of 37.6 $W\,m^{-1}$. Dotted line: simulated temperature oscillation amplitude vs frequency due to the silicon substrate only with the assumption of an infinite resistance at the bottom of the sample. Dashed line: simulated amplitude of a silicon wafer covered with a 570-nm-thick silica layer, ■: experimental points. The difference between the dotted line and the experimental points corresponds to the temperature drop through the SiO_2 layer.

conductivity. At frequencies above 40 Hz, the WPD is shorter than the strip width; the thermal wave is then confined near the metal line. The experimental phase shift is in between the two calculated curves neglecting and taking into account the heater thickness, respectively. This suggests that the thermal properties of the heater disturb the temperature profile in the sample and will be discussed in the next part.

Figure 5 also demonstrates the sensitivity of the simulation, regarding the phase shift. An excellent agreement is observed between the calculated curves and the experimental data: in the two extreme regimes, low- and high-frequency, calculations using appropriate assumptions allow the data to be interpreted. If the thermal properties of the heater are neglected, the calculated phase shift (dotted line) tends to be $-\pi/4$ at high frequencies. This is consistent with Eq. (2) when analyzing it at a high frequency (solid line).[30]

The comparison of calculation and experiment on the SiO_2/Si sample is illustrated in Fig. 6. The system under consideration consists of a 230-μm-thick silicon wafer covered with a thermally grown 570-nm-thick silica layer. Measurements of the temperature oscillation amplitude from the ac heating were performed between 10 and 1000 Hz. Figure 6 shows the experimental data for the metal strip deposited directly on the SiO_2 film, simulated curves for the SiO_2/Si system, and the contribution of the Si substrate alone to the temperature oscillation amplitude. An adiabatic boundary condition at the bottom of the sample was assumed.

The agreement between the simulated and experimental results is fairly good in the whole frequency range based on literature values for the thermal conductivity of bulk Si and SiO_2. The value of 1.4 $W\,m^{-1}\,K^{-1}$ used for silica is in excellent agreement with previous results.[7,31] At low frequencies (below 100 Hz), as seen previously, the finite thickness of the silicon is responsible for the deviation from the linear dependence (the WPD exceeds the width of the substrate). However, in this case, the silicon grease introduces a thermal resistance between the Si substrate and the sample holder, leading to an increase of the temperature oscillation amplitude at the heater. As expected, the silica layer introduces a frequency-independent thermal resistance. The thermal conductivity of the silica layer, extracted from this figure by means of Eq. (5) supports also the value used in the simulation.

C. Effect of a finite strip thickness

The previous section has shown that both the experimental results and numerical simulations deviate from Eq. (2) even at frequencies high enough so that boundary conditions do not have to be considered. The reason is that Cahill's derivation ignores transverse heat flow and heat capacitance of the heater. By varying the thermal properties of the heater in our simulation, i.e., the thermal conductivity and the heat capacity of the heater, it is possible to appreciate the role of these two parameters in the two extreme regimes of frequency. Several conclusions can be drawn from the simulations performed on the Kapton system.

We observed that at low and high frequencies the temperature amplitude oscillation is lower and the phase shift higher than those predicted by Eq. (2), whatever the thermal properties of the heater. At low frequency, the decrease of the temperature amplitude can be seen as a decrease in the constant η in Eq. (4). In this regime, the thermal mass of the heater can be neglected because the WPD is far larger than the heater thickness: the heater is in a quasisteady state regime. η then is a function of the thermal conductivity and the heater geometry only. The heat spreading arises because of the nonhomogeneous temperature along the width of the heater.

At high frequency, the conclusions are different. The amplitude of the complex temperature rise is constant along the width of the heater at each time and therefore there is no transverse heat flow in the heater. The amplitude is not a function of the thermal conductivity of the heater but of its heat capacity, its geometry and frequency. The heater's heat capacity and thermal conductivity can then be measured individually by choosing the appropriate frequency.

VI. CONCLUSION

A heat conduction model for the 3ω method based on the finite volume technique has been developed. The simulation is free from binding hypotheses and completes the numerical approaches first developed by Cahill.[18] The possibilities of the numerical simulations coupled to the experiment to analyze the experimental data and extract the thermal conductivity by fitting, have been demonstrated. The simulation appears as a powerful tool for predicting which geometry of the heater strip and which range of frequency are the most suitable to analyze a given system by means of analytical formulas. We hope that the simulation developed in this study will contribute to the analyzing of systems exhibiting a low thermal conductivity contrast as well as to extracting the thermal conductivities of anisotropic materials.

ACKNOWLEDGMENTS

The authors would like to thank D. Song and T. Borca-Tasciuc for discussions and critical reading of the manuscript.

[1] G. Chen, J. Heat Transfer **119**, 220 (1997).
[2] G. Chen and M. Neagu, Appl. Phys. Lett. **71**, 2761 (1997).
[3] G. Chen, Phys. Rev. B **57**, 14958 (1998).
[4] A. Balandin and K. L. Wang, Phys. Rev. B **58**, 1544 (1998).
[5] R. Venkatasubramanian, Phys. Rev. B **61**, 3091 (2000).
[6] D. G. Cahill, M. Katiyar, and J. R. Abelson, Phys. Rev. B **50**, 6071 (1994).
[7] S. M. Lee and D. G. Cahill, J. Appl. Phys. **81**, 2590 (1997).
[8] S. M. Lee, D. G. Cahill, and R. Venkatasubramanian, Appl. Phys. Lett. **70**, 2957 (1997).
[9] D. G. Cahill, S. M. Lee, and T. I. Selinder, J. Appl. Phys. **83**, 5783 (1998).
[10] G. Chen, S. Q. Zhou, D. Y. Yao, C. J. Kim, X. Y. Zheng, Z. L. Liu, and K. L. Wang, Proc. 17th Intern. Conf. on Thermoelectrics, Nagoya, Japan, 1998, p. 202.
[11] T. Borca-Tasciuc *et al.*, Mater. Res. Soc. Symp. Proc. **545**, 473 (1999).
[12] A. J. Griffin, Jr., F. R. Brotzen, and P. J. Loos, J. Appl. Phys. **75**, 3761 (1994).
[13] X. Zhang and C. P. Grigoropoulos, Rev. Sci. Instrum. **66**, 1115 (1995).
[14] S. Govorkov, W. Ruderman, M. W. Horn, R. B. Goodman, and M. Rothschild, Rev. Sci. Instrum. **68**, 3828 (1997).
[15] D. M. Bhusari, C. W. Teng, K. H. Chen, S. L. Wei, and L. C. Chen, Rev. Sci. Instrum. **68**, 4180 (1997).
[16] G. B. M. Fiege, A. Altes, R. Heiderhoff, and L. J. Balk, J. Phys. D **32**, L13 (1999).
[17] M. L. Grilli, D. Ritsau, M. Dieckmann, and U. Willamowski, Appl. Phys. A: Mater. Sci. Process. **71**, 71 (2000).
[18] D. G. Cahill, Rev. Sci. Instrum. **61**, 802 (1990).
[19] D. G. Cahill and R. O. Pohl, Phys. Rev. B **35**, 4067 (1987).
[20] S. Huxtable, A. Shakouri, P. Abraham, Y. J. Chiu, X. Fan, J. E. Bowers, and A. Majumdar, Proc. 18th Intern. Conf. on Thermoelectrics, Baltimore, MD, 1999, p. 594.
[21] D. Song, C. Caylor, W. L. Liu, T. Zeng, T. Borca-Tasciuc, T. D. Sands, and G. Chen, Proc. 18th Intern. Conf. on Thermoelectrics, Baltimore, MD, 1999, p. 679.
[22] Y. S. Ju, K. Kurabayashi, and K. E. Goodson, Thin Solid Films **339**, 160 (1999).
[23] U. G. Jonsson and O. Andersson, Meas. Sci. Technol. **9**, 1873 (1998).
[24] A. Jacquot, M. Stölzer, J. Meusel, O. Boffoue, B. Lenoir, and A. Dauscher, Proc. Fifth European Workshop on Thermoelectrics, Pardubice, 1999, p. 31.
[25] A. M. James and M. P. Lord, *Macmillan's Chemical and Physical Data*, (Macmillan, London, 1992).
[26] Y. S. Touloukian, R. W. Powell, C. Y. Ho, and P. G. Klemens, *Thermophysical Properties of Matter*, The TPRC Data Series Vols. 1 and 2 (IFI/Plenum, New York, 1970).
[27] Y. S. Touloukian and E. H. Buyco, *Thermophysical Properties of Matter*, The TPRC Data Series Vols. 4 and 5 (IFI/Plenum, New York, 1970).
[28] Kapton polyimide: General Specification, Dupont.
[29] M. Von Arx, O. Paul, and H. Baltes, J. Microelectromech. Syst. **9**, 136 (2000).
[30] I. K. Moon, Y. H. Jeong, and S. I. Kwun, Rev. Sci. Instrum. **67**, 29 (1996).
[31] H. H. Kim, A. Feldman, and D. Novotny, J. Appl. Phys. **86**, 3959 (1999).